Research Square

Preprints are preliminary reports that have not undergone peer review.
They should not be considered conclusive, used to inform clinical practice,
or referenced by the media as validated information.

Disorder Induced Quantum Griffiths Phase in the Proximate Kitaev Quantum Spin Liquid Na2Co2TeO6

Wassilios Papawassiliou

wassilios.papawassiliou@ens-lyon.fr

Centre de la Research Scientifique https://orcid.org/0000-0002-3698-3593

Nicolas Lazardis

NCSR Demokritos / NTUA Athens

Eunice Mumba Mpanga

Institut Charles Gerhard Montpellier

Jonas Koppe

Centre de la Research Scientifique / Centre de RMN à Très Hauts Champs de Lyon

Nikolaos Panopoulos

National Center for Scientific Research "Demokritos"

Lydia Gkoura

BRC, Technology Innovation Institute

Romain Berthelot

Institut Charles Gerhard Montpellier

Michael Fardis

National Center for Scientific Research "Demokritos"

Gaël De Paëpe

Université Grenoble Alpes, CEA, IRIG, MEM

Andrew Pell

ENS Lyon https://orcid.org/0000-0002-2542-8113

Georgios Papavassiliou

NCSR Demokritos https://orcid.org/0000-0002-4119-3959

Article

Keywords:

Posted Date: August 12th, 2026

DOI: https://doi.org/10.21203/rs.3.rs-10266479/v1

License: This work is licensed under a Creative Commons Attribution 4.0 International License.
Read Full License

Additional Declarations: There is **NO** Competing Interest.

Disorder Induced Quantum Griffiths Phase in the Proximate Kitaev Quantum Spin Liquid $Na_2Co_2TeO_6$

Wassilios Papawassiliou[1]*, Nicolas Lazaridis[2,3], Eunice Mumba Mpanga[4], Jonas Koppe[1], Nikolaos Panopoulos[2], Lydia Gkoura[5], Romain Berthelot[4], Michael Fardis[2], Gaël De Paëpe[6], Andrew J. Pell[1,7], and Georgios Papavassiliou[2]*

Affiliations [1] Centre de RMN à Très Hauts Champs de Lyon (UMR 5280 CNRS / ENS Lyon / Université Claude Bernard Lyon 1), Université de Lyon, 5 rue de la Doua, 69100 Villeurbanne, France

[2] Institute of Nanoscience and Nanotechnology, National Center for Scientific Research "Demokritos", 153 10 Aghia Paraskevi, Attiki, Greece

[3]School of Applied Mathematical and Physical Sciences, National Technical University of Athens, 15780 Zografou, Athens, Greece

[4]ICGM, Univ Montpellier, CNRS, ENSCM, Montpellier 34095, France

[5]BRC, Technology Innovation Institute, PO Box 9639, Masdar City, Abu Dhabi, UAE

[6]Université Grenoble Alpes, CEA, IRIG, MEM, Grenoble 38000, France

[7]Institut Universitaire de France (IUF)

*Corresponding authors: wassilios.papawassiliou@ens-lyon.fr, g.papavassiliou@inn.demokritos.gr

Disorder is generally expected to destabilize a Kitaev quantum spin liquid, yet it can also generate new quantum phases. $Na_2Co_2TeO_6$, which contains substantial intrinsic Na-site disorder, provides a promising platform to examine how randomness reshapes spin dynamics. Here, by employing ^{23}Na NMR, we reveal a disorder induced softening of the spin excitations. Between 10 K and 100 K, the temperature dependence of the NMR relaxation times is consistent with the presence of gapped fractional spin excitations. Below 10 K, however, they bifurcate into two distinct channels: a slow-relaxing channel, preserving the gapped excitations character, and a fast-relaxing channel that follows a Korringa-like law, indicating the emergence of nearly gapless spin excitations. This two-channels regime is accompanied by ultraslow, microsecond-scale spin fluctuations following an Arrhenius activation law. Besides, ab initio NMR lineshape calculations show that a quantum spin liquid-like model reproduces the low-temperature NMR spectra sufficiently better than magnetically ordered models. Together, our findings indicate transition upon cooling to a disorder-driven quantum spin liquid Griffiths phase, comprising slowly fluctuating gapped regions within a matrix of nearly gapless low-energy spin excitations.

Topological quantum matter encompasses systems in which fundamentally new collective phenomena emerge from quantum entanglement rather than spontaneously broken symmetries. A paradigmatic example is the Kitaev honeycomb model, in which local spins fractionalize into itinerant Majorana fermions moving in a background of localized Z_2 gauge fluxes (visons)[1,2]. In a magnetic field, this fractionalized state becomes gapped and enters a chiral, non-Abelian quantum spin liquid (QSL) phase with topologically protected edge modes[2,3]. Yet the central challenge is not simply to identify materials proximate to the Kitaev limit, but to determine what genuinely new physics survives once the ideal model is realized in a real crystal, where magnetic order, lattice-scale imperfections and random bond perturbations inevitably compete with topological coherence.

So far, experimental access to this regime has been dominated by 4d and 5d spin-orbit-assisted honeycomb magnets such as α-$RuCl_3$ [4–7] and α-$(Na,Li)_2IrO_3$ [8,9]. These materials established the modern phenomenology of proximate Kitaev magnetism, but they also exposed its fragility: residual Heisenberg exchange, off-diagonal anisotropies and quenched disorder typically drive the system into long-range magnetic order, most commonly zigzag antiferromagnetism[10–12]. As a result, even when broad excitation continua appear in inelastic neutron scattering[5] and the NMR spin-lattice relaxation time constant T_1 displays the characteristic temperature dependence associated with fractionalized spin dynamics[6,7], the ground state is generally interpreted as proximate to a Kitaev QSL rather than a direct realization of it. This raises a broader question of high current interest: can disorder do more than destabilize the Kitaev state, and instead generate qualitatively new forms of fractionalized matter unavailable in the clean limit?

Among candidate Kitaev magnets, $Na_2Co_2TeO_6$ (NCTO) is especially compelling because it brings this question into an experimentally accessible 3d transition metal system. Here, Co^{2+} ions in the $3d^7$ configuration form a honeycomb lattice and realize spin-orbit-entangled pseudospin moments, $J_{eff} = 1/2$, with pronounced bond-directional interactions, placing the material close to the Kitaev exchange limit where fractionalized excitations are expected[13,14]. Like the 4d/5d candidates, NCTO is considered to order antiferromagnetically below $T_N \approx 27$ K, and was initially discussed in terms of zigzag order[13–19]. More recent neutron results, however, show that its ground state is a noncollinear triple$-q$ structure that preserves the crystal C_3 symmetry[20–22], consistent with proximity to a hidden $SU(2)$-symmetric point characterized by nearly degenerate multi-q states and a sizeable Kitaev exchange, $K \approx -8.29$ meV ($\sim$100 K)[22]. This already places NCTO at an unusual position between frustration, accidental degeneracy and strong bond-anisotropic exchange. Crucially, it also hosts intrinsic Na-site occupation disorder[23], offering a natural route to random bond perturbations in a material that is simultaneously close to a Kitaev QSL. NCTO therefore provides an opportunity not merely to test for proximate spin-liquid behavior above T_N, akin to the "Kitaev paramagnet" regime of α-$RuCl_3$ [6,7], but to ask whether disorder and field can jointly reorganize the low-energy sector into a

distinct fractionalized regime. Direct experimental evidence for such disorder-driven randomization of the Co-O-Co geometry and the associated exchange couplings, however, has so far remained lacking.

Here we show that NCTO realizes disorder-tuned fractional spin dynamics and that randomness is not merely a perturbation, but an organizing principle of the low-temperature state. Using ^{23}Na solid-state nuclear magnetic resonance (NMR) from 3 to 300 K in magnetic fields of 4.7 T and 9.4 T, we identify three signatures of disorder-enabled spin fractionalization. First, in the range $T \sim 100 - 10$ K, the spin-lattice relaxation rate $1/T_1$ follows a concave temperature dependence characteristic of field-induced gapped Kitaev excitations. Second, below 10 K, the relaxation splits into two channels: a slow component that preserves the gapped fractionalized response, and a fast component that obeys a Korringa-like law, $1/(T_1T) = ct$, revealing the emergence of nearly gapless low-energy excitations. Third, this heterogeneous two-spin-fluid regime is accompanied by ultraslow microsecond spin fluctuations with Arrhenius-type activation. Together, these observations point to a regime in which gapped and nearly gapless fractional excitations coexist in real space.

Ab initio ^{23}Na NMR lineshape calculations on a DFT-relaxed NCTO supercell with realistic random Na occupancy directly support this interpretation. DFT calculations show, first, that the relaxed Co-O-Co bond angles and Co-O bond lengths of edge-sharing octahedra are distributed over $\sim 3 - 4$ % around their mean values, naturally generating spatially random Kitaev exchange couplings; and second, that only a Kitaev QSL model reproduces the experimental low-temperature NMR powder patterns, whereas zigzag and triple$-q$ antiferromagnetic states do not. These results indicate that under an applied external magnetic field the low-temperature response is dominated not by a conventional ordered texture, but by a QSL-like state whose character is fundamentally reshaped by disorder.

Taken together, our results point to the emergence of a Kitaev-Griffiths regime in the Z_2 gauge-flux sector, in line with recent theoretical predictions[24]. In this picture, randomly distributed Na vacancies locally distort Co-O-Co bonds and disrupt the spatial uniformity of the underlying Kitaev state, producing a mosaic of vison-rich, nearly gapless regions intertwined with vison-poor, gapped islands of fractional excitations. This framework, on the one hand, explains why the topological spin-liquid phase is so fragile in real materials. On the other hand, it shows that disorder can generate new emergent physics rather than simply destroying the clean-limit state: a dynamically heterogeneous, Griffiths-type fractionalized phase in which robust low-energy excitations survive and even dominate.

^{23}Na NMR crystallography reveals a Kitaev QSL ground state in NCTO

To investigate the evolution of the magnetic interactions in NCTO with temperature, we employed magic-angle-spinning (MAS) and static solid-state ^{23}Na NMR lineshape measurements across a broad temperature range (3-300 K). Subsequently, by considering the various proposed spin configurations, the low temperature experimental NMR spectra were compared with spectral

parameters derived from *ab initio* calculations. This "NMR crystallography" approach provides a robust framework for assessing the underlying magnetic interactions.

Figure 1a presents the room temperature ^{23}Na MAS NMR spectrum acquired at 9.4 T and a MAS frequency of 60 kHz. The observed sideband manifold spans 3000 ppm, with an asymmetric envelope centered at ~685 ppm. To analyze the sideband pattern, a Bessel-series model was used (see Suppl. Note 2), accounting for both isotropic and anisotropic shifts as well as quadrupolar interactions. The analysis revealed two inequivalent Na sites, with resonances at $\delta_{iso} \approx 700 \pm 50$ ppm for Na(1) (orange line) and 180 ± 30 ppm for Na(2) (red line), with an integral ratio of ~6: 1, consistent with the XRD Rietveld refinement (Suppl. Fig. S1 and Suppl. Table S1). Accurate spectral fitting requires incorporating broad distributions of isotropic NMR shifts (insert in Fig. 1a), indicating significant variability in Na-Co distances and supporting a model of partial disorder in Na-site occupation.

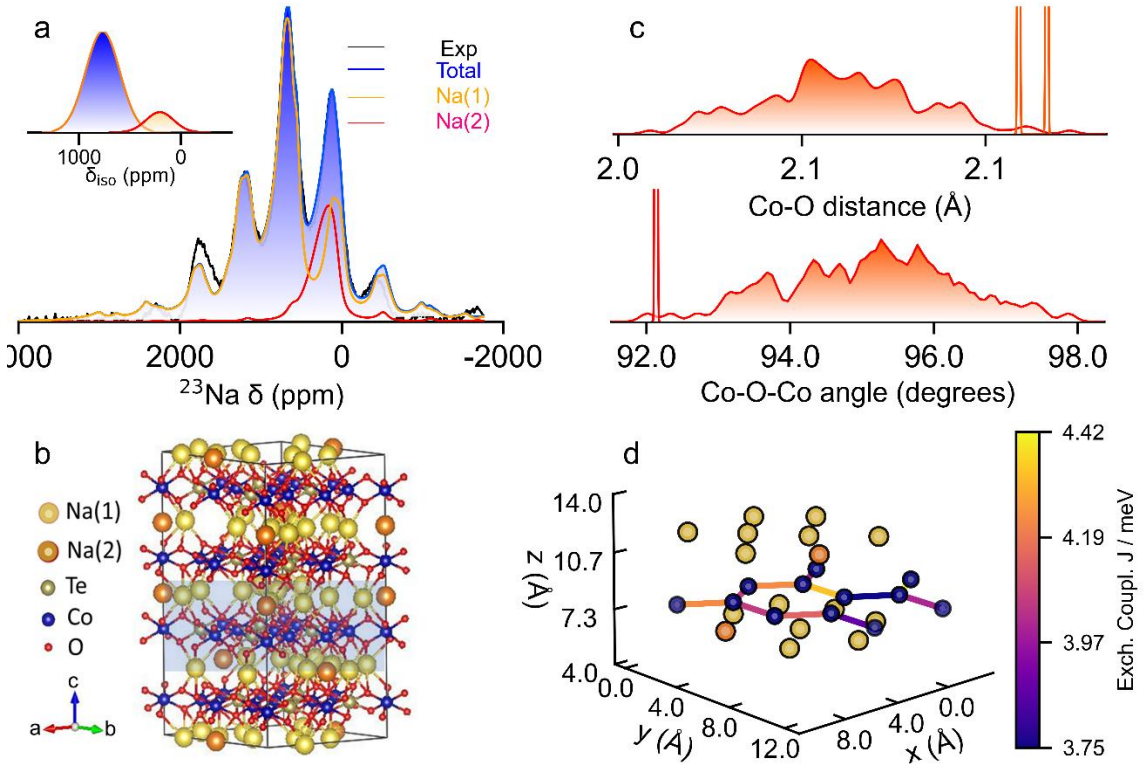


Figure 1 | Na disorder randomizes Kitaev exchange couplings in $Na_2Co_2TeO_6$. a, ^{23}Na MAS NMR spectrum (black line) recorded at room temperature under a 9.4 T magnetic field at spinning rate of 60 kHz. The orange and red lines display the fitted Na(1) and Na(2) components, centered at $\delta_{iso} \approx 700 \pm 50$ ppm and 180 ± 30 ppm, respectively, with integral ratio $I_{Na(1)}/I_{Na(2)} \approx 6$. The inset shows broad isotropic shift δ_{iso} distribution for both Na sites, signifying substantial variation in the Na-Co distances. **b,** Representation of a 2×2×2 NCTO supercell, showing honeycomb CoO_6/TeO_6 layers (blue, red, gold spheres) and disordered Na(1)/Na(2) layers (yellow/orange spheres), consistent with NMR based experimental occupancies. **c,** Distribution of Co-O-Co angles and Co-O bond lengths in edge sharing octahedra, within the honeycomb layers of the NCTO supercell, before (sharp orange lines) and after

(broad red lines) DFT relaxation. **d,** Co honeycomb layer at z = 8.42 Å in the relaxed NCTO supercell (blue shaded layer), with bonds color-coded according to calculated Kitaev's exchange couplings, revealing random variation attributable to Na disorder.

Based on these findings, a 2x2x2 supercell of NCTO was constructed, incorporating randomly distributed Na(1) and Na(2) sites according to the NMR derived occupancies (Fig. 1b). After full structural relaxation using density functional theory (DFT), all in-plane nearest-neighbor Co-Co pairs and their bridging oxygen atoms were examined. For each Co-O-Co linkage, the two Co-O distances (d_1, d_2) and the bond angle θ were determined, with the effective Co-O distance defined as $r = (d_1 + d_2)/2$. As shown in Fig. 1c, based on experimental X-ray diffraction, the unrelaxed structure displays uniform delta-function like r and θ distributions (sharp orange lines). In contrast, the DFT-relaxed structure (red lines) leads to a broad distribution of both parameters (red lines), reflecting a substantial distribution of both r and θ, with median values $r_0 \approx 2.05\,\AA$, and $\theta_0 \approx 95°$.

To quantify the impact of the structural disorder on the magnetic interactions, the Kitaev exchange coupling constant was calculated using the phenomenological expression $K = K_{\max}[1 - c(\theta - \theta_0)^2](\frac{r_0}{r})^p$, with $K_{\max}$ set according to recent theoretical predictions as $K_{\max} \approx 9$ meV[22] and $p \approx 10$ [26,27], as explained in Suppl. Note 3. This approach relies on two well-established facts: (i) the pronounced Co-O-Co angular dependence of superexchange interactions across the edge-sharing octahedra, with bond-anisotropic Kitaev interactions peaked between $90° - 100°$ [8,28,29]. The quadratic angular dependence in the above expression provides a compact means of encoding deviations from the optimal geometry, consistent with theoretical calculations. (ii) The rapid suppression of orbital-overlap-mediated exchange couplings with increasing metal-ligand distance, which here is parameterized by a power law with exponent $p \approx 10$.

Application of this model to the relaxed NCTO supercell reveals variation of up to $\sim 30\%$ in the Kitaev exchange coupling constants. This bond-to-bond randomness is visualized in Fig. 1d, where Co-Co links are color-coded by their calculated K values, highlighting the emergence of random-bond Kitaev physics, apparently driven by Na disorder.

To elucidate how Na disorder influences the evolution of the magnetic interactions with temperature, static ^{23}Na NMR lineshape measurements were performed over the range 3-300 K. Data collected at 9.4 T are shown in Fig. 2a. At temperatures above a characteristic threshold $T^* \sim 100$ K, the spectra are broad and symmetric, consistent with Curie-Weiss paramagnetism. Below this temperature, the lineshapes develop a pronounced low-frequency tail, indicative of emerging short-range correlations in which antiferromagnetic (AFM) or Kitaev interactions partially counteract the conventional ^{23}Na paramagnetic shift. This crossover is consistent with previous reports of correlated paramagnetic behavior at low applied fields [18]. Notably, at temperatures below 30 K, the NMR spectra evolve into broad single-peaked Gaussians, lacking the typical trapezoidal shape seen in collinear AFM powder patterns[30]. This result is consistent with the absence of $1/T_1$ critical divergence across all temperature,

as shown in Fig. 3b, confirming that under strong magnetic fields, such as 9.4 T, the transition from the PM to the AFM state is suppressed[17,21].

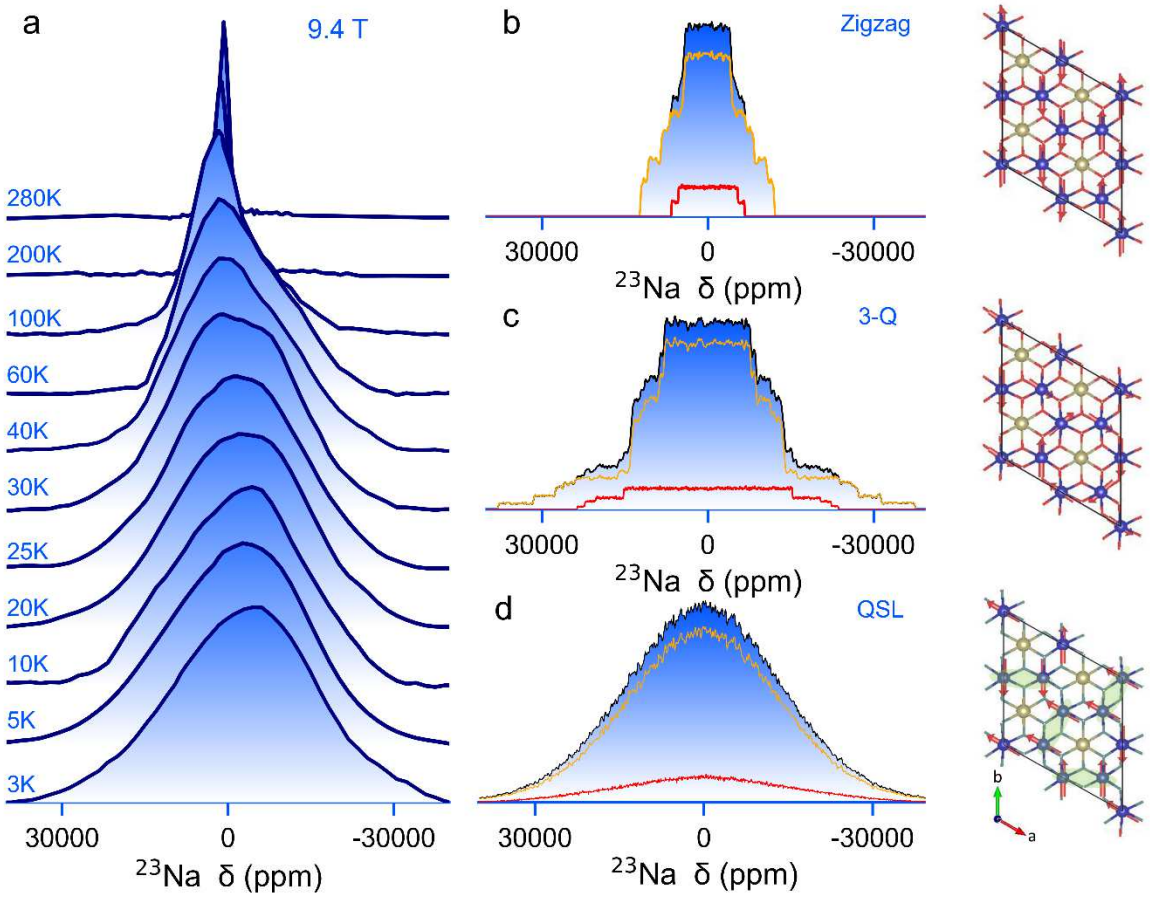


Figure 2 | Static ^{23}Na NMR lineshapes identify a QSL ground state. a, Temperature dependence of the ^{23}Na NMR spectra from 300 K to 3 K at 9.4 T. **b–d,** Ab-initio simulated NMR powder patterns for the zigzag AFM, triple-q AFM, and QSL spin textures at 9.4 T, utilizing a DFT-relaxed 2x2x2 supercell with random Na occupancy as a template. The depicted spin-configurations at the right side pertain to the second Co layer of the supercell. Out of the three spin-configurations, only the QSL model reproduces the shape and width of the experimental spectrum at low temperatures. Yellow and red lines represent contributions from Na(1) and Na(2), respectively.

To identify the low-temperature spin configuration, we performed ab initio calculations of static ^{23}Na NMR powder patterns for the three most widely discussed candidate states: zigzag AFM, triple AFM, and QSL. Each model was mapped onto the DFT-relaxed NCTO supercell (Figs. 2b-d). For every Na nucleus, the dipolar hyperfine shift δ_{dip} and the second-order quadrupolar shift δ_{quad} were calculated for 10,000 random orientations of the external magnetic field, yielding a total shift $\delta_{tot} =$

$\delta_{dip} + \delta_{quad}$ for each direction. However, the quadrupolar contribution was found to be only a minor correction. The resulting simulated spectra are shown in Figs. 2b-d, with additional details, especially for the QSL state, provided in Supplementary Note 4.

The zigzag AFM state produces a central plateau corresponding to the Yamada-Sakata feature[30] commonly observed in collinear AFM systems, although the predicted width is substantially smaller than that observed experimentally at 3 K. The triple$-q$ AFM state yields broader edges but still retains plateau-like features that are absent from the experimental spectra. By contrast, the QSL model, constructed as a superposition of Kitaev-like bond-directional spin configurations within each Co layer of the NCTO supercell and evaluated over the 10,000 magnetic field orientations, reproduces with striking accuracy both the shape and the exceptionally large $\sim$40,000 ppm static linewidth of the experimental ^{23}Na NMR spectrum at 3 K. This agreement indicates that, under a 9.4 T magnetic field at low temperature, NCTO is more faithfully described by a highly degenerate QSL-like spin state than by a static antiferromagnetic configuration. A similar temperature evolution of the NMR lineshapes was observed at 4.7 T (Supplementary Fig. S4a). Although long-range AFM order sets in at $T_N \approx 27$ K, the low-temperature NMR profiles remain broad, single-peaked, and nearly Gaussian, closely resembling those measured at 9.4 T. This observation rules out a pure zigzag AFM ground state at 4.7 T, despite its frequent assignment in the literature[19].

It should be noted that alternative spin configurations, such as random two-dimensional spin freezing within the *ab* plane, could also account for the pronounced low-temperature NMR line broadening, as shown in Suppl. Figure S5a. In a spin-glass scenario, however, one would expect strong wipeout of the NMR signal upon cooling due to severe shortening of the spin-spin relaxation time T_2, as well as a magnetic-field dependence of the spin-lattice relaxation time T_1 with temperature - features that are not observed in NCTO.

Spin-lattice relaxation reveals coexistence of gapped and gapless fractional excitations below 10 K

While ^{23}Na NMR lineshape measurements primarily probe the static spin configuration, the temperature dependence of the spin-lattice relaxation rate $1/T_1$ provides direct insight into the underlying spin dynamics. To probe these dynamics, extensive T_1 measurements were performed over the temperature range of 3 K to 300 K in two representative magnetic fields: (i) at 9.4 T, where according to the literature long-range AFM order is suppressed[17,21], and (ii) at 4.7 T, where NCTO is reported to undergo a paramagnetic-to-antiferromagnetic (PM-AFM) transition at $T_N \approx 27$ K.

Upon cooling from room temperature, in the temperature range ~100 K to 10 K, the system enters into a dynamically uniform phase, dominated by fractional spin excitations, as demonstrated below. At lower temperatures, NCTO exhibits a dynamically heterogeneous state characterized by two significantly broadened NMR relaxation channels. This phenomenon is clearly illustrated in Fig. 3a, showing representative low-temperature ^{23}Na NMR T_1 distributions at 9.4 T. Between 50 K and 20 K,

the distributions remain largely unchanged: however, further cooling leads to rapid broadening. Below 10 K, a second prolonged component emerges, with both relaxation channels displaying considerable broadening spanning more than four orders of magnitude.

The temperature dependence of T_1 at 9.4 T is summarized in the $1/T_1$ vs T plot shown in Figure 3b. Upon cooling from room temperature, $1/T_1$ reduces rapidly, reaching a shallow minimum at $\sim$100 K, followed by a gradual increase that culminates in a broad maximum around 40 K, yielding a characteristic concave temperature profile. Such behavior has previously been reported in $RuCl_3$ and attributed to gapped Kitaev fractional spin excitations [7]. No critical divergence in $1/T_1$ is observed upon crossing T_N, implying the absence of a PM-AFM phase transition, in agreement with prior studies conducted under strong magnetic fields[17,21]. Notably, Quantum-Monte-Carlo calculations for $1/T_1$ in the Kitaev honeycomb model (open green circles), adapted from ref.[31] with appropriate temperature rescaling, show excellent agreement with the experimental data points (yellow squares).

The dominance of fractional spin excitations is further supported by the excellent fit to the empirical law

$$\frac{1}{T_1} \propto \frac{1}{T} e^{-\left(\frac{n\Delta}{T}\right)} \qquad (1),$$

originally used to describe NMR relaxation in the presence of fractional spin excitations in $RuCl_3$[7] (see also Suppl. Fig. S3a). Fitting Eq. (1) to the experimental points (with $n = 0.67$)[7] an excitation gap of $\sim$35 K is obtained. The simultaneous agreement with both the QMC simulation and Eq. (1) provides compelling evidence that the intermediate-temperature regime is dominated by gapped Majorana quasiparticles.

On cooling below $\sim$10 K, the single $1/T_1$ branch splits into two distinct relaxation components, as illustrated in Fig. 3b. The slow-relaxing component (yellow squares) extrapolates smoothly from the high temperature curve, indicative of regions dominated by gapped fractional excitations. However, the fast-relaxing component (blue squares) varies linearly with temperature, a hallmark of gapless spin excitations in a Fermi-liquid-like bath[24,25], that is analogous to the Korringa law in metallic systems[32]. When replotted as $1/T_1T$ versus T (Fig. 3c), below 10 K it saturates to a constant value ~ 0.0052 $K^{-1}ms^{-1}$, while the slow component remains exponentially suppressed. This Korringa-like behavior has been theoretically predicted as the hallmark of a Griffiths phase in the bond-disordered Kitaev honeycomb model[24,25], where random exchange couplings close the flux gap, generating a continuum of low-energy states, and eventually zero-energy Majorana modes[33–35].

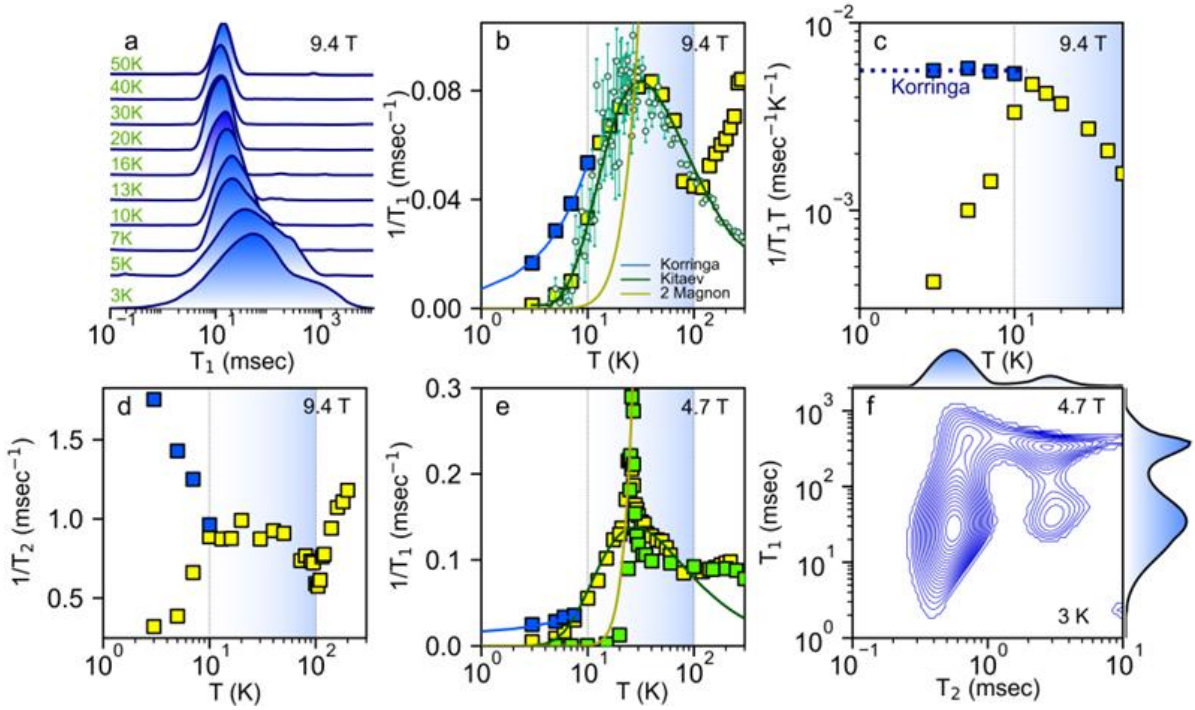


Figure 3 | T_1 evidence of heterogeneous fractional spin dynamics in NCTO. a, ^{23}Na T_1 distributions at 9.4 T between 50 K and 3 K. Below 10 K, the distributions broaden markedly and an additional long-T_1 component emerges. **b,** Temperature dependence of $1/T_1$ at 9.4 T. Experimental data (yellow squares) are compared with quantum Monte Carlo results for the Kitaev model (open green circles, ref. 31). The dark green line is a fit to Eq. (1), the dark yellow line corresponds to the two-magnon model (Eq. 2), and the blue line is linear fit illustrating $1/T_1 \propto T$. **c,** $1/(T_1T)$ versus temperature, highlighting the Korringa-like behavior of the fast T_1 component (blue squares). **d,** Temperature dependence of the transverse relaxation rate $1/T_2$ at 9.4 T. **e,** $1/T_1$ versus temperature at 4.7 T (blue/yellow squares). For comparison, $1/T_1$ data for the zigzag antiferromagnet $Na_2Ni_2TeO_6$ (ref. 36) are shown as green squares. Dark green, brown and blue lines are fits as in panel b. **f,** T_1–T_2 correlation spectrum at 3 K, displaying diffuse rectangular contours and anti-diagonal cross-peaks, indicative of entangled relaxation channels.

At 4.7 T, NCTO reveals the PM-AFM phase transition, marked by a sharp peak in the $1/T_1$ versus T curve at $T_N \approx 27$ K (Fig. 3e, Suppl. Fig S4b), in agreement with earlier ^{23}Na NMR studies[18,37]. Remarkably, upon entering the ordered phase, $1/T_1$ retains the same concave temperature dependence observed at 9.4 T and remains well described by Eq. (1). This unusual behavior is further emphasized by comparison with the structurally analogous $Na_2Ni_2TeO_6$ (NNTO)[36], which instead follows the conventional two-magnon relaxation mechanism expected for ordered antiferromagnets[38] (green squares in Fig. 3e),

$$1/T_1 \propto T^2 \exp(-\Delta/T) \qquad (2).$$

On further cooling below ~10 K, $1/T_1$ at 4.7 T again bifurcates into two components (Fig. 3e), reproducing the dual relaxation channels seen at 9.4 T, with the slower branch continuing to follow

Eq. (1) down to the lowest measured temperature. Finally, to rule out sample-dependent effects, earlier T_1 datasets collected at 5 T and 8 T in previous work[37] were re-examined; their consistency with Eq. (1) (Suppl. Fig. S3b) confirms that the low temperature spin-dynamics in NCTO are generically governed by QSL-like fractional excitations.

It should also be noted that the experimental $1/T_1$ data for the slow-relaxing component at the two magnetic fields fall onto a single curve over the entire low-temperature regime, as shown in Supplementary Fig. S5b. This magnetic field independence is incompatible with conventional spin-glass freezing, in which the $1/T_1$ relaxation maximum is expected to shift markedly by varying the magnetic field, as illustrated in Suppl. Fig. S5b and discussed in Suppl. Note 5.

Transverse relaxation and ultraslow spin dynamics

The crossover from the conventional high-temperature PM state into the Kitaev paramagnet is likewise captured in the transverse NMR relaxation channel. At 9.4 T, the spin–spin relaxation rate $1/T_2$ exhibits a pronounced minimum at $T^* \approx 100$ K (Fig. 3d), marking the onset of the Kitaev-dominated dynamics. Because ^{23}Na is a quadrupolar nucleus, a quadrupolar Carr–Purcell–Meiboom–Gill (qCPMG) sequence was employed[39], as described on top of Suppl. Fig. S6. The resulting spin-echo decays were inverted to yield the T_2 distributions (Fig. 4a). Between 100 K and 10 K, data are well described by a single relaxation component, yielding relatively narrow T_2 distributions (Figs. 4c,4d). In this regime, $1/T_2$ varies only weakly with temperature, closely mirroring the behavior of $1/T_1$. At 4.7 T, however, a sharp divergence of $1/T_2$ is observed at T_N, reflecting the critical slowing down at the PM–AFM transition (inset, Fig. 4c).

Upon cooling below $\sim$10 K, the T_2 distributions broaden dramatically and split into two components (Figs. 4a,b), in direct correspondence with the dual relaxation channels identified in T_1. Notably, their temperature dependences are strikingly different: in the slow-relaxing channel, $1/T_2$ decreases on cooling, consistent with the Kitaev-type relaxation mechanism that governs the gapped $1/T_1$ branch. In contrast, the fast-relaxing T_2 channel shows a relatively steep upturn as $T \to 0$ (inset, Fig. 4c). Within the general spin-spin relaxation formalism, $1/T_2 = \gamma_n^2 \langle B_z^2 \rangle \tau_c \propto \chi^2(T)\, \tau_c$, where γ_n is the nuclear gyromagnetic ratio, $\langle B_z^2 \rangle$ the mean-square amplitude of longitudinal field fluctuations[40], and τ_c the spin-fluctuations correlation time. The observed behavior can thus be considered as combination of a power-law susceptibility, $\chi(T) \sim T^{-\alpha}$, expected for random-exchange interactions[24,41], and the concomitant growth of τ_c upon cooling.

The relationship between the T_1 and T_2 relaxation channels is clearly illustrated in the two-dimensional T_1–T_2 correlation spectrum at 3 K in magnetic field of 4.7 T (Fig. 3f). The contour plots reveal two prominent diagonal components, with double-peaked projections along each axis. The short-T_2 signal component corresponds to the short-T_1 component, that is assigned to gapless fractional

excitations, whereas the long-T_2 component corresponds to the long-T_1, that is characterized by gapped fractional excitations. Notably, the contours reveal strong cross-diagonal peaks, indicating a subtle entanglement between the two relaxation channels. An analogous pattern is observed at 9.4 T (Suppl. Fig. S7), indicating that this heterogeneous dynamics is an intrinsic property of NCTO rather than a field-dependent effect.

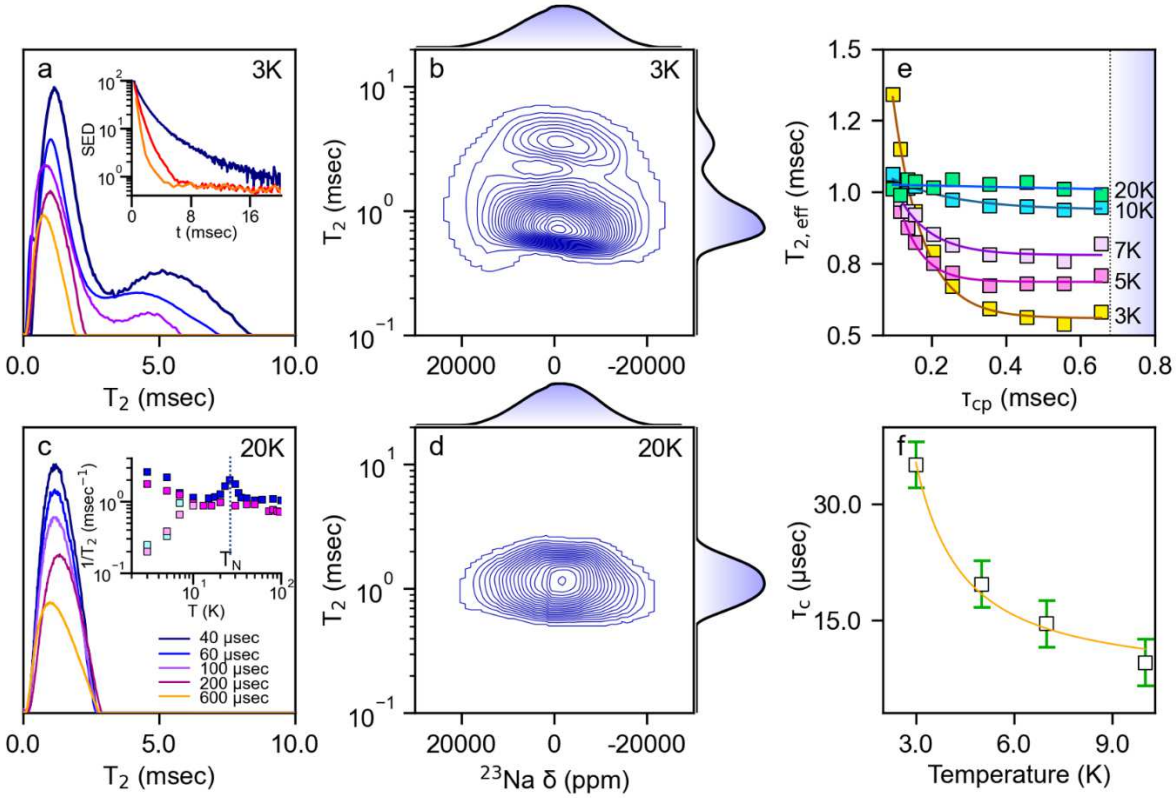


Figure 4 | Ultraslow spin dynamics from T_2 relaxation. a, ^{23}Na NMR T_2 distributions in 9.4 Tesla at 3 K for various τ_{cp} values, obtained by inverting the SEDs acquired using a q-CPMG pulse sequence (illustrated on top of the Figure). The inset shows representative SEDs corresponding to different τ_{cp} values. An increase in τ_{cp} suppresses the long T_2 component. **b,** Frequency-resolved T_2 distribution as a function of frequency at 3 K with τ_{cp}= 40 μs. **c,** T_2 distributions at 20 K across different τ_{cp} values. For $T > 10$ K, distributions are unimodal and independent of τ_{cp}. The inset displays $1/T_2$ versus T at 4.7 T (blue and cyan squares) and 9.4 T (dark and light magenta squares). **d,** Frequency-resolved T_2 distribution at 20 K for τ_{cp}= 40 μs. **e,** The effective $T_{2,eff}$ as a function of τ_{cp} at various temperatures, with fits to Eq. (3). **f,** Correlation time τ_c versus T, fitted to an Arrhenius activation law.

A striking manifestation of ultraslow spin dynamics - an essential hallmark of a Griffiths phase[42,43] - is revealed by the dependence of T_2 on the time interval τ_{cp} separating consecutive pulses in the q-CPMG pulse sequence, as defined in Suppl. Fig. S7. For $T < 10$ K, increasing τ_{cp} causes the long-T_2 component to shift rapidly to shorter values and diminish in intensity, vanishing entirely for

$\tau_{cp} > 200$ μs (Figs. 4a, 4b Suppl. Fig. S6). By contrast, for $T > 10$ K, T_2 remains independent of τ_{cp} (Figs. 4c–4e, Suppl. Fig. S6), consistent with the collapse of the slow component.

To quantify this behavior, Fig. 4e shows the effective spin–spin relaxation time, $T_{2,eff}$, extracted from the initial slope of the spin-echo decays as a function of τ_{cp} at various temperatures. For $T < 10\,K$, the data are accurately represented by

$$T_{2,eff} = [\,\tau_c\langle S^2(0)\rangle\{1 - (\tfrac{\tau_c}{\tau_{cp}})tanh(\tfrac{\tau_{cp}}{\tau_c})\}]^{-1} \qquad (3),$$

an expression originally developed to describe ultraslow chemical exchange in spin-1/2 nuclei[44] and later applied to the lateral diffusion of quadrupolar nuclei along curved membrane surfaces[45]. In the present context, the dominant relaxation channel arises from electron-spin fluctuations, mediated by dipolar electron-nuclear interactions and characterized by an exponentially decaying autocorrelation function, $\langle S(t)S(0)\rangle = \langle S^2(0)\rangle e^{-t/\tau_c}$. Here, τ_c denotes the correlation time of the spin fluctuations and $\langle S^2(0)\rangle$ their squared amplitude. Further details on Eq. (3) can be found in Suppl. Note 7.

The dependence of T_2 on τ_{cp} thus provides direct evidence for the presence of ultraslow spin fluctuations in the microsecond timescale. Crucially, the extracted correlation times τ_c follow an Arrhenius law, $\tau_c = \tau_0 exp(U/k_B T)$, with an activation energy $U/k_B \approx 4.9$ K and a pre-exponential factor $\tau_0 \approx 13.8$ μs (Fig. 4f). A comparable trend is observed at 4.7 T, although the weaker intensity of the slow component at the lowest temperatures precludes a precise determination of the activation energy.

Fractional excitations in a Griffiths QSL phase

A comprehensive understanding of our results hinges on the nature of fractional excitations in a Kitaev QSL and their coupling to structural disorder. In the disorder-free limit, spin degrees of freedom fractionalize into itinerant, gapless Majorana fermions and localized, gapped $\mathbb{Z}_2$ fluxes (visons)[2,3]. Application of a magnetic field hybridizes these sectors, opening a topological gap $\Delta \propto B^3$and stabilizing a chiral, non-Abelian K-QSL[3].

In NCTO, however, by combining ^{23}Na NMR lineshape measurements with ab initio calculations, we show that Na-vacancy disorder actively induces bond randomness rather than simply being a passive distortion. The DFT-relaxed NCTO supercell demonstrates that random Na occupancy leads to up to ~3% variations in nearest-neighbor Co-O bond lengths and Co-O-Co angles, corresponding to ~30% fluctuations in Kitaev exchange couplings. This structural randomness directly seeds the heterogeneous spin dynamics observed in both T_1 and T_2.

In this context, disorder is not a secondary correction, but it fundamentally reshapes the low-energy density of states $\rho(E)$. Numerical studies predict that vacancy- and bond-disordered Kitaev models replace the sharp vison gap with a power-law continuum, $\rho(E) \propto E^{-\alpha}$with $0 < \alpha < 1$[33–35], giving rise to Griffith-phase dynamics. Three key hallmarks characterize this regime: (i) power-law

thermodynamics[33–35], (ii) a Korringa-like NMR relaxation channel[24,25], and (iii) scale-invariant spin dynamics[46]. Our relaxation data align precisely with this scenario. Between 100 K and 10 K, $1/T_1$ follows the activated form expected for gapped Kitaev excitations with $\Delta \approx 35$K. Below ~10 K, however, the relaxation bifurcates into two branches: a slow branch, retaining the gapped fractional character, while the fast branch follows a Korringa law, $1/T_1T = ct$, as predicted in the strong-disorder Griffiths regime[24,25]. The exceptionally broad T_1 distributions and the emergence of ultraslow microsecond-scale fluctuations, governed by an Arrhenius barrier of $U/k_B \approx 5$K, further attest to rare-region physics, establishing disorder as a generative mechanism for emergent fractionalized dynamics.

Comparable coexistence of gapped and gapless relaxation channels has been reported in $H_3LiIr_2O_6$[47]. Crucially, the slow-relaxing component in NCTO originates not from isolated singlets, as in the case of $H_3LiIr_2O_6$, but from extended islands of gapped fractional dynamics, persisting down to the lowest temperatures.

In summary, our ^{23}Na NMR results indicate that sodium disorder induces local distortions in the Co-O bonds and Co-O-Co angles, randomizing Co-Co exchange interactions. This destabilizes the topologically uniform vison sector, resulting in a mosaic of gapless, vison-rich regions interspersed with gapped, vison-poor islands. While the low temperature NMR lineshape measurements are in favor of a Kitaev-QSL, the T_1 and T_2 analysis reveal the dynamic signature of a Griffiths-phase as the framework of the QSL state. At 4.7 T, the observed AFM transition at $T_N \approx 27$ K reflects the emergence of AFM patches, however, below 10 K the quantum Griffiths-phase appears to also dominate at this weaker external magnetic field.

Methods

Sample preparation and characterization. The $Na_2Co_2TeO_6$ polycrystalline sample was synthesized using a solid-state reaction method. Initially, stoichiometric amounts of Na_2CO_3 (Alfa, 99.95%), Co_3O_4 (prepared by calcining $CoCO_3$ (Alfa Aesar, 99%) at 400°C for 15 hours), and TeO_2 (Thermo Scientific, 99.99%) were mixed with a 5% excess of Na_2CO_3 and thoroughly ground. The mixture was then loaded into a gold boat, inside an alumina crucible and sintered at 900 °C in air for 12 hours. The resulting product was then ground into a fine powder, and its phase purity was confirmed using X-ray diffraction (XRD) analysis.

XRD characterization. XRD spectra were obtained with an analytical PANalytical X'Pert PRO powder diffractometer, utilizing Cu-Kα radiation (λ = 1.5418 Å) with an applied voltage of 40 kV and intensity of 30 mA. The spectra were collected in the angular range (2θ) of 5–80° with a step size of 0.03°. The obtained XRD data was further analyzed through Rietveld refinement using the FULLPROF software program, providing structural parameters and confirming the hexagonal crystal structure of $Na_2Co_2TeO_6$ in the space group P6322. The unit cell parameters were determined to be a = b = 5.274 Å, c = 11.239

Å, and the volume of the unit cell was calculated to be 270.7701 $Å^3$. The XRD analysis confirmed the formation of a pure $Na_2Co_2TeO_6$ phase, with diffraction peaks indexed to indicate the crystalline structure's integrity.

NMR measurements. ^{23}Na MAS NMR experiments on the NCTO polycrystalline material were performed with a 1.3 mm HXY triple-resonance probe, at 60 kHz MAS on a Bruker 400 Avance-III spectrometer operating at a ^{23}Na Larmor frequency of 105.87 MHz. Spectral acquisition was done with a rotor synchronized Hahn-echo sequence with a Central Transition-selective 0.8 μs 90° excitation pulse. 65536 signal transients were accumulated with a repetition time of 20ms.

The frequency-sweep ^{23}Na NMR spectra were acquired on two home-built NMR spectrometers under static conditions, equipped with two superconducting magnets operating at magnetic fields 4.7 Tesla and 9.4 Tesla. For the spin-lattice relaxation time T_1, the spin-spin relaxation time T_2 experiments, and the relevant $T_1 - T_2$ experiments, a π/2-t-π/2 saturation recovery pulse sequence and a q-CPMG pulse sequence $\pi/2\text{-}\tau_{cp}/2\text{-}\{\pi/2\text{-}\tau_{cp}\text{-}\pi/2\}_N$ with a train of N=300 π/2 pulses and appropriate phase cycling were implemented (Suppl. Figs. S6-S9). The T_1 and T_2 distribution analysis was performed by applying a non-negative Tikhonov Regularization Algorithm, as described in Suppl. Note 6. Given that ^{23}Na is an $I = 3/2$ quadrupolar nucleus, analysis of the saturation recovery curves by selectively irradiating the central transition (+1/2 ↔ -1/2) was performed based on the relation $(M_0 - M)/M_0 = \{0.1\exp(-t/T_1) + 0.9\exp(-6t/T_1)\}$[18,35].

Author contributions. W.P., and G.P. conceived and designed the experiments and did most of the paper writing (with contribution from all coauthors). ^{23}Na MAS NMR and analysis was performed by W.P., A.J.P., and G.D.P. Frequency sweep static ^{23}Na NMR and relaxation experiments were performed by N.L., M.F., N.P, and L.G. NMR relaxation analysis was performed by W.P., J.K., G.P., and A.J.P. Sample preparation and characterization were performed by E.M.M., R.B.

Acknowledgments. N.L. would like to thank Professor A. Kontos from the NTUA-Greece for the academic support during his Master Thesis. W.P. and A.J.P. were supported by the Agence Nationale de la Recherche (ANR-21-CE29-0010-01"MatPNMR"). A.J.P. received additional support from the Institut Universitaire de France (IUF). J.K. was funded by the European Union's Horizon Europe research and innovation programme under the Marie Sklodowska-Curie grant agreement No 101111472 "ParaMAS". G.D.P. was supported by the French National Research Agency (ANR-19-CE29-0021 and ANR17-EURE-0003 through the LabEx Arcane ANR-15-IDEX-02).

Competing Interests statement. Authors declare that they have no competing interests.

Additional Information. Supplementary Information is included in the SI document. This includes, Supplementary Notes, Supplementary Figs. S1 to S7, and Supplementary Table S1.

References

1. Nayak, C., Simon, S. H., Stern, A., Freedman, M. & Das Sarma, S. Non-Abelian anyons and topological quantum computation. *Rev. Mod. Phys.* **80**, 1083-1159 (2008).
2. Kitaev, A. Yu. Fault-tolerant quantum computation by anyons. *Ann. Phys.* **303**, 2-30 (2003).
3. Kitaev, A. Anyons in an exactly solved model and beyond. Ann. *Phys.* **321**, 2-111 (2006).
4. Plumb, K. W. *et al.* α-$RuCl_3$: A spin-orbit assisted Mott insulator on a honeycomb lattice. *Phys. Rev. B* **90**, 041112 (2014).
5. Banerjee, A. *et al.* Neutron scattering in the proximate quantum spin liquid α-$RuCl_3$. *Science* **356**, 1055-1059 (2017).
6. Baek, S.-H. *et al.* Evidence for a Field-Induced Quantum Spin Liquid in α-$RuCl_3$. *Phys. Rev. Lett.* **119**, 037201 (2017).
7. Janša, N. *et al.* Observation of two types of fractional excitation in the Kitaev honeycomb magnet. *Nat. Phys.* **14**, 786–790 (2018).
8. Jackeli, G. & Khaliullin, G. Mott Insulators in the Strong Spin-Orbit Coupling Limit: From Heisenberg to a Quantum Compass and Kitaev Models. *Phys. Rev. Lett.* **102**, 017205 (2009).
9. Chun, S. H., *et al.* Direct evidence for dominant bond-directional interactions in a honeycomb lattice iridate Na_2IrO_3. *Nat. Phys.* **11**, 462–466 (2015).
10. Johnson, R. D. *et al.* Monoclinic crystal structure of α-$RuCl_3$ and the zigzag antiferromagnetic ground state. *Phys. Rev. B* **92**, 235119 (2015).
11. Chaloupka, J., Jackeli, G. & Khaliullin, G. Zigzag Magnetic Order in the Iridium Oxide Na_2IrO_3. *Phys. Rev. Lett.* **110**, 097204 (2013).
12. Singh, Y. & Gegenwart, P. Antiferromagnetic Mott insulating state in single crystals of the honeycomb lattice material Na_2IrO_3. *Phys. Rev. B* **82**, 064412 (2010).
13. Songvilay, M. *et al.* Kitaev interactions in the Co honeycomb antiferromagnets $Na_3Co_2SbO_6$ and $Na_2Co_2TeO_6$. *Phys. Rev. B* **102**, 224429 (2020).
14. Kim, C. *et al.* Antiferromagnetic Kitaev interaction in $J_{eff} = 1/2$ cobalt honeycomb materials $Na_3Co_2SbO_6$ and $Na_2Co_2TeO_6$. *J. Phys. Condens. Matter* **34**, 045802 (2022).

15. Jiao, J. *et al.* Static magnetic order with strong quantum fluctuations in spin-1/2 honeycomb magnet $Na_2Co_2TeO_6$. *Commun. Mater.* **5**, 159 (2024).
16. Lefrançois, E. *et al.* Magnetic properties of the honeycomb oxide $Na_2Co_2TeO_6$. *Phys. Rev. B* **94**, 214416 (2016).
17. Lin, G. *et al.* Field-induced quantum spin disordered state in spin-1/2 honeycomb magnet $Na_2Co_2TeO_6$. *Nat. Commun.* **12**, 5559 (2021).
18. Lee, C. H. *et al.* Multistage development of anisotropic magnetic correlations in the Co-based honeycomb lattice $Na_2Co_2TeO_6$. *Phys. Rev. B* **103**, 214447 (2021).
19. Bera, A. K., Yusuf, S. M., Kumar, A. & Ritter, C. Zigzag antiferromagnetic ground state with anisotropic correlation lengths in the quasi-two-dimensional honeycomb lattice compound $Na_2Co_2TeO_6$. *Phys. Rev. B* **95**, 094424 (2017).
20. Chen, W. *et al.* Spin-orbit phase behavior of $Na_2Co_2TeO_6$ at low temperatures. *Phys. Rev. B* **103**, L180404 (2021).
21. Bera, A. *et al.* Field-induced phase transitions and anisotropic magnetic properties of the Kitaev-Heisenberg compound $Na_2Co_2TeO_6$. *Phys. Rev. B* **108**, 214419 (2023*)*.
22. Krüger, W. G. F., Chen, W., Jin, X., Li, Y. & Janssen, L. Triple-q Order in $Na_2Co_2TeO_6$ from Proximity to Hidden-SU(2)-Symmetric Point. *Phys. Rev. Lett.* **131**, 146702 (2023).
23. Viciu, L. *et al.* Structure and basic magnetic properties of the honeycomb lattice compounds $Na_2Co_2TeO_6$ and $Na_3Co_2SbO_6$. *J. Solid State Chem.* **180**, 1060-1067 (2007).
24. Dantas, V. & Andrade, E. C. Disorder, Low-Energy Excitations, and Topology in the Kitaev Spin Liquid. *Phys. Rev. Lett.* **129**, 037204 (2022).
25. Nasu, J. & Motome, Y. Spin dynamics in the Kitaev model with disorder: Quantum Monte Carlo study of dynamical spin structure factor, magnetic susceptibility, and NMR relaxation. *Phys. Rev. B* **104**, 035116 (2021).
26. Goodenough, J. *Magnetism and the Chemical Bond*. (John Wiley And Sons, 1963).
27. Harrison, W. *Electronic Structure and the Properties of Solids: The Physics of the Chemical Bond*. (San Francisco: Freeman, 1980).

28. Winter, S. *et al.* Models and materials for generalized Kitaev magnetism. *J. Phys. Condens. Matter.* **29**, (2017).

29. Liu, H. & Khaliullin, G. Pseudospin exchange interactions in d^7 cobalt compounds: Possible realization of the Kitaev model. *Phys. Rev. B* **97**, (2018).

30. Yamada, Y. & Sakata, A. An Analysis Method of Antiferromagnetic Powder Patterns in Spin-Echo NMR under External Fields. *J. Phys. Soc. Jpn.* **55**, 1751-1758 (1986).

31. Nasu, J. Majorana quasiparticles emergent in Kitaev spin liquid. *Prog. Theor. Exp. Phys.* **2024**, 08C104 (2024).

32. Korringa, J. Nuclear magnetic relaxation and resonance line shift in metals. *Physica* **16**, 601-610 (1950).

33. Knolle, J., Moessner, R. & Perkins, N. B. Bond-Disordered Spin Liquid and the Honeycomb Iridate $H_3LiIr_2O_6$: Abundant Low-Energy Density of States from Random Majorana Hopping. *Phys. Rev. Lett.* **122**, 047202 (2019).

34. Kao, W.-H., Knolle, J., Halász, G. B., Moessner, R. & Perkins, N. B. Vacancy-Induced Low-Energy Density of States in the Kitaev Spin Liquid. *Phys. Rev. X* **11**, 011034 (2021).

35. Kao, W.-H. & Perkins, N. B. Disorder upon disorder: Localization effects in the Kitaev spin liquid. *Ann. Phys.* **435**, 168506 (2021).

36. Itoh, Y. ^{23}Na Nuclear Spin-Lattice Relaxation Studies of $Na_2Ni_2TeO_6$. *J. Phys. Soc. Jpn.* **84**, 064714 (2015).

37. Kikuchi, J. *et al.* Field evolution of magnetic phases and spin dynamics in the honeycomb lattice magnet $Na_2Co_2TeO_6$: ^{23}Na NMR study. *Phys. Rev. B* **106**, 224416 (2022).

38. Beeman, D. & Pincus, P. Nuclear Spin-Lattice Relaxation in Magnetic Insulators. *Phys. Rev.* **166**, 359-375 (1968).

39. Abragam, A. *The Principles of Nuclear Magnetism*. (Oxford Univ. Press, 2011).

40. Slichter, C. P. *Principles of Magnetic Resonance*. vol. 1 (Springer, 1990).

41. Kimchi, I., Sheckelton, J. P., McQueen, T. M. & Lee, P. A. Scaling and data collapse from local moments in frustrated disordered quantum spin systems. *Nat. Commun.* **9**, 4367 (2018).

42. Volta, T., & Schmalian, J. Quantum Griffiths effects in itinerant Heisenberg magnets. *Phys. Rev. B* **72**, 045438 (2005).

43. Li, Y., *et al.* Spin dynamics and Griffiths singularity in the random quantum Ising magnet $PrTiNbO_6$ *npj Quantum Mater.* **6**, 34 (2021).

44. Luz, Z. & Meiboom, S. Nuclear Magnetic Resonance Study of the Protolysis of Trimethylammonium Ion in Aqueous Solution-Order of the Reaction with Respect to Solvent. *J. Chem. Phys.* **39**, 366-370 (1963).

45. Bloom, M. & Sternin, E. Transverse nuclear spin relaxation in phospholipid bilayer membranes. *Biochemistry* **26**, 2101–2105 (1987).

46. Yamada, M. G. Anderson-Kitaev spin liquid. *npj Quantum Mater.* **5**, 82 (2020).

47. Lee, C. *et al.* Coexistence of random singlets and disordered Kitaev spin liquid in $H_3LiIr_2O_6$. *Phys. Rev. B* **107**, 014424 (2023).

Supplementary Files

This is a list of supplementary files associated with this preprint. Click to download.

- NCTOSI.pdf